TECHNISCHE MECHANIK, Band 22, Heft 4, (2002), 247-258
Manuskripteingang: 13. Dezember 2001

Numerical Dispersion Error in Finite Methods, Exemplified by the Perfectly Straight Beam Undergoing Bending Oscillations [1]

O. Weckner, G. Brunk

In chapter (1) we present numerical simulations of the eigenstates of a MBS-model (Multi-Body-System) for a continuous ring structure. Both eigenfrequencies and eigenforms show a systematic error for high mode numbers. In order to understand the source of this error, in chapter (2) we calculate analytical solutions for the eigenfrequencies of a MBS- and a FEM-model (Finite-Element-Method) for the straight beam undergoing bending oscillations. We summarize our results in chapter (3).

1 Introduction

This paper presents a summary of our contribution at the CIMRF '01 in Berlin.

The mathematical description of continua is often based on partial differential equations (PDE) which in general have to be solved numerically. Finite methods such as FDS (Finite-Difference-Scheme), FEM or MBS projects a continuum (with infinite degrees of freedom) on a discrete system (with finite degrees of freedom). The question arises under what circumstances these two systems can be substituted. In order to answer this question, it is useful to compare the corresponding frequency spectra which we obtained analytically for a concrete system in chapter (2). On the other hand, some of these discrete systems can actually be materialized by means of MBS-systems. Therefore there are two interpretations of the results obtained in this chapter.

When analyzing experimental data, one usually distinguishes between randomly spread errors and systematic errors caused by the instruments and methods used. Using discrete models for continuous systems, there are also two sources of error: rounding errors and a systematic error depending on the discretization method used. For example, longitudinal mass-spring-chains in mechanics as a model for an oscillating bar (or four-pole-chains in electrodynamics as a model for real cables) show an artificial dispersion compared to the corresponding continuous systems which inherit no dispersion. One can show that one gets identical results when using FDS to solve the wave equation that describes these systems.

In this paper we analytically investigate the distribution of eigenfrequencies in two discretization methods for the straight beam undergoing bending oscillations: MBS and FEM. As this continuous systems inherit natural dispersion, we expect to find additional numerical dispersion. The paper is based particularly on Brunk and Weckner (2001) and Weckner (2000).

[1] Contribution to the sixth conference "Current Ideas in Mechanics, Thermodynamics, and Related Fields (CIMRF 2001)", Sept. 3-6, 2001, TU Berlin

In Weckner (2000), plane bending oscillations of a ring are investigated with the following MBS-model, supported at node 1:

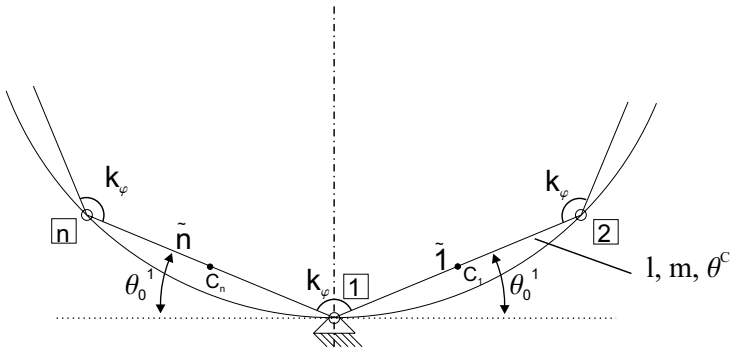

Figure 1: MBS-Model of a Ring and Boundary Conditions

For a number of 64 bars (i.e. a degree of freedom of 62) the 8th eigenmode looks like this:

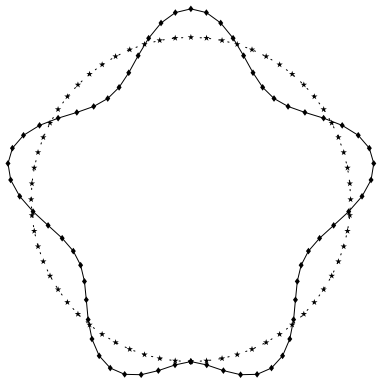

Figure 2: 8th Eigenmode of a Ring, $\tilde{n} = 64$

By increasing the number of bars, the discrete model approaches the ring geometry in the undeformed state. By choosing appropriate parameters we expect the dynamic behaviour of our model to be similar to the behaviour of the continuous ring. This is indeed so for frequencies reasonably smaller than the highest eigenfrequency of the discrete model. When plotting the frequency spectrum, the lines approaching this highest eigenfrequency are compressed:

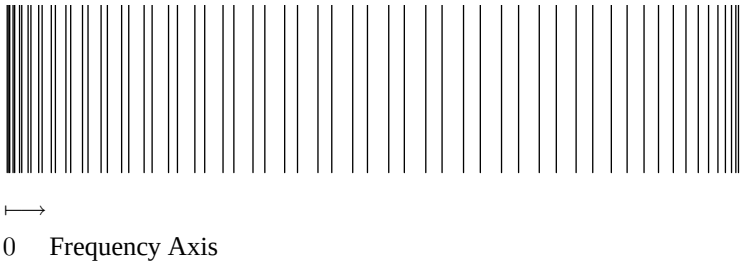

Figure 3: Frequency Spectrum of the Ring, $\tilde{n} = 64$

For the continuous beam, the gap between two adjacent eigenfrequencies should get wider because the influence of specific boundary conditions becomes negligible for higher modes and eventually, the eigenfrequencies become proportional to the square of the mode (similar to the free ring where this can be shown analytically, see Weckner (2000)). This compression effect of the discontinuum will be called *numerical dispersion*. (The compression near the smallest frequency can also be found for the continuous ring and is not an influence of discretization.)

Another way of presenting the eigenfrequencies is to plot the modal density distribution:

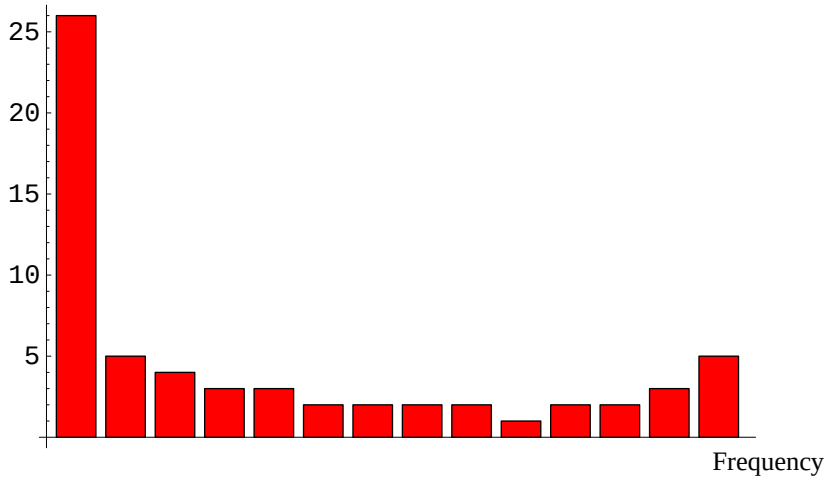

Figure 4: Modal Density Distribution of the Ring, $\tilde{n} = 64$

Here the total frequency range (difference of highest and lowest eigenfrequency) was divided in 14 equidistant intervals, and the number of eigenfrequencies in each interval was counted and plotted over the frequency axis. Again, the compression at both ends of the spectrum can be observed.

One could be tempted to interpret this effect as a speciality of the MBS model of the ring under the given boundary conditions. In Weckner (2000) it is demonstrated that a similar compression occurs for other boundary conditions and for a geometry differing from the ring as well. But also the method of discretization is not the source for this compression, as a FEM simulation will demonstrate.

So far, all results were based on numerical simulations. That is why in Brunk and Weckner (2001) we obtained some analytical solutions for an MBS model of the straight beam undergoing bending oscillations.

The results so far lead to the following assumption: whenever the infinite degrees of freedom of a continuous system are ”approximated” by a finite number, numerical dispersion occurs, regardless of the specific continuum investigated, its boundary conditions or the discretization method used. This is a well known phenomenon, as a literature research confirmed, e.g. Cherukuri (1999), Rao et al. (1999) or Brepta et al. (1994). As far as the authors know, all papers so far used numerical simulations to demonstrate that a concrete discretization method applied to a continuous system produces numerical dispersion. In distinction, this paper presents analytical solutions of two discretization methods for a continuum, thus giving a mathematical proof for this compression effect. It should be seen as a step on the way to understand and estimate this discretization error which can become serious when high frequency problems of continua are solved numerically using finite methods.

2 Analytical Solutions for Two Discrete Models of the Perfectly Straight Beam Undergoing Bending Oscillations

The most simple one-dimensional continua are governed by the (homogeneous) wave equation: $\ddot{\eta}(x,t) - c^2\eta''(x,t) = 0$ (e.g. longitudinal oscillations of a beam, with wave velocity $c = \sqrt{\frac{E}{\rho}}$, with E, the modulus of elasticity (YOUNGs modulus) and ρ, the mass density). The discretization technique commonly used for this non-dispersive mechanical system is a mass-spring-chain which is basically a MPS (Mass-Point-System) model. For common boundary conditions, there exist analytical solutions for the eigenfrequencies for a given number of elements.
In electrical engineering, the same mathematical theory is known as the wave parameter form of four-poles used to analyze the behaviour of real cables and lines, see Brillouin (1953) and Rint (1981).
It is interesting to notice that these originally non-dispersive continua become dispersive upon discretization. In Brunk and Weckner (2001), we transferred this well-known theory to more complex continua possessing natural dispersion such as the perfectly straight beam undergoing bending oscillations. There are a number of assumptions made in the classical theory of beams performing bending oscillations. The most important assumptions are the following: we use a linearized theory for the shear rigid, linear elastic BERNOULLI-beam with negligible rotational inertia and no normal forces, resulting in the following PDE:

$$K_B w^{iv}(x,t) + m_x \ddot{w}(x,t) = q(x,t), \tag{1}$$

where K_B is the bending stiffness, m_x the mass per unit length and q(x,t) the vertical force per unit length. Let L be the length of the beam. Choosing boundary conditions that specify the moment as well as the displacement on both ends to be zero, there exist exact analytical solutions for the eigenfrequencies,

$$\begin{aligned} \omega_m^E &= \pi^2 \sqrt{\frac{K_B}{m_x L^4}}\, m^2 \\ m &= 1, 2, \ldots, \infty. \end{aligned} \tag{2}$$

which are exactly proportional to the square of the mode.

2.1 MBS Discretization

The next step is the discretization. For a smooth limiting process, the beam is divided into $\tilde{N}$ *equidistant* elements:

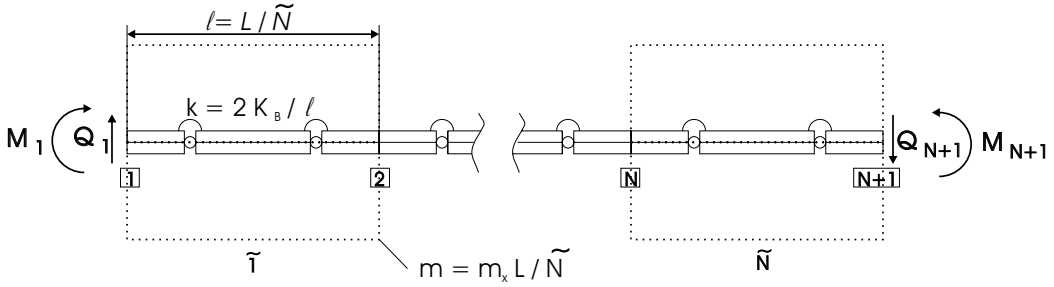

Figure 5: Topology of the MBS Chain

The parameters (ℓ, m, k) of one element are chosen to be consistent with the parameters (L, m_x, K_B) of the continuum for the case $\tilde{N} \to \infty$.

In the next graphic, the displacement and interior (generalized) forces (shear force Q, bending moment M) are shown:

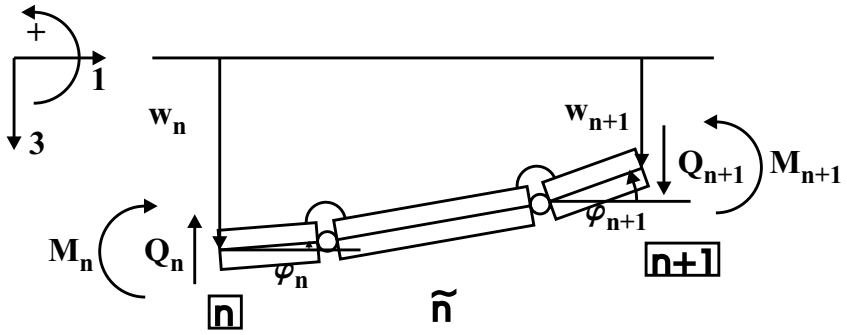

Figure 6: State of Displacement and Generalized Forces

The degree of freedom of this element is 4 if one subtracts the degree of freedom associated with longitudinal displacement. It is reasonable to do so because in a first order theory of the straight beam, longitudinal and vertical oscillations are uncoupled.
For the $\tilde{n}$-th element we chose the following coordinates:

$$\mathbf{q}_n = (w_n,\ \ell\varphi_n,\ w_{n+1},\ \ell\varphi_{n+1})^T\ . \tag{3}$$

By calculating the kinetic and potential energy one easily finds the equation of motion for the element:

$$\mathbf{M}_{MBS}\ddot{\mathbf{q}}_n + \mathbf{K}_{MBS}\mathbf{q}_n = \mathbf{F}_e\ . \tag{4}$$

Here the mass and stiffness matrix ($\mathbf{M}_{MBS},\ \mathbf{K}_{MBS}$) of the element and the generalized forces ($\mathbf{F}_e$) acting on the element - internal with respect to the entire beam and external with respect to the element being cut free - are:

$$\mathbf{M}_{MBS} = m\begin{pmatrix} 5/12 & -7/96 & 1/12 & 1/48 \\ -7/96 & 1/64 & -1/48 & -1/192 \\ 1/12 & -1/48 & 5/12 & 7/96 \\ 1/48 & -1/192 & 7/96 & 1/64 \end{pmatrix}, \tag{5}$$

$$\mathbf{K}_{MBS} = \frac{k}{\ell^2}\begin{pmatrix} 8 & -4 & -8 & -4 \\ -4 & 5/2 & 4 & 3/2 \\ -8 & 4 & 8 & 4 \\ -4 & 3/2 & 4 & 5/2 \end{pmatrix}, \tag{6}$$

$$\mathbf{F}_e = (-Q_n,\ -\frac{M_n}{\ell},\ Q_{n+1},\ \frac{M_{n+1}}{\ell})^T. \tag{7}$$

Now we start assuming a harmonic solution: $\mathbf{q}_n = \hat{\mathbf{q}}_n\ e^{i\omega t} + \hat{\mathbf{q}}_n^*\ e^{-i\omega t}$. This leads to the definition of the dynamical stiffness matrix:

$$\mathbf{K} := \mathbf{K}_{MBS} - \omega^2\mathbf{M}_{MBS} =: \begin{pmatrix} \mathbf{K}_{1,1} & \mathbf{K}_{1,2} \\ \mathbf{K}_{2,1} & \mathbf{K}_{2,2} \end{pmatrix}\ :\ \mathbf{K}\mathbf{q}_n = \mathbf{F}_e\ . \tag{8}$$

Obviously, $\mathbf{K}$ is a 4x4 matrix. With regard to the introduction of the transfer matrix later on it will be useful to define the 4 submatrices $\mathbf{K}_{i,j}$ of dimension 2x2. $\mathbf{M}_{MBS},\ \mathbf{K}_{MBS}$ (and in consequence, $\mathbf{K}$) are symmetric due to the derivation from the kinetic and potential energy and real-valued as a consequence of vanishing friction.

Next, we define the state vector of the n-th node as:

$$\mathbf{z}_n = (w_n,\ \ell\varphi_n, -\frac{\ell^2}{k}\ Q_n,\ -\frac{\ell}{k}\ M_n)^T\ . \tag{9}$$

By introducing the transfer matrix **T** (which does not depend on the node because of the homogeneity along the beam),

$$\mathbf{T} = \begin{pmatrix} -K_{1,2}^{-1}K_{1,1} & \frac{k}{\ell^2}K_{1,2}^{-1} \\ -\frac{\ell^2}{k}(K_{2,1} - K_{2,2}K_{1,2}^{-1}K_{1,1}) & -K_{2,2}K_{1,2}^{-1} \end{pmatrix}, \tag{10}$$

the state at node n+1 can be expressed in terms of the state at node n and the transfer matrix:

$$\mathbf{z}_{n+1}(t)\ = \mathbf{T}(\eta)\mathbf{z}_n(t) \tag{11}$$

$$\eta := \frac{\omega}{\omega_c},\ \omega_c = \sqrt{\frac{1536}{5}}\ \sqrt{\frac{k}{m\ell^2}}\ . \tag{12}$$

The frequency ω is normalized with the smallest non-zero eigenfrequency of the free element. Using the topological symmetry of the element (see Brunk and Weckner, 2001) the inverse transfer matrix reads

$$\mathbf{T}^{-1} = \mathbf{DTD} \text{ with} \tag{13}$$

$$\mathbf{D} = \begin{pmatrix} 1 & 0 & 0 & 0 \\ 0 & -1 & 0 & 0 \\ 0 & 0 & -1 & 0 \\ 0 & 0 & 0 & 1 \end{pmatrix}\ .$$

From (10) and (13) one can deduce the following: if λ_i is an eigenvalue of T and $\mathbf{z}_i^E$ the corresponding eigenvector, then $1/\lambda_i$ is also an eigenvalue to the corresponding eigenvector $\mathbf{Dz}_i^E$.
A more general proof for this can be found in Brunk and Weckner (2001).
Next, the eigenvalues λ_i and eigenvectors $\mathbf{z}_i^E$ $(i = 1,\ \ldots,\ 4)$ of **T** are calculated. The roots of the characteristic polynomial of **T**,

$$P[\lambda] \quad = \quad \text{Det}[\mathbf{T} - \lambda\mathbf{I}] = \text{Det}[\lambda^2\mathbf{K}_{1,2} + \lambda(\mathbf{K}_{1,1} + \mathbf{K}_{2,2}) + \mathbf{K}_{2,1}]\ /\ \text{Det}[\mathbf{K}_{1,2}] \tag{14}$$

as well as the eigenvectors can be found analytically, see Brunk and Weckner (2001). The visualization of the eigenvalues as a function of the frequency η shows that the first (and consequently, the second) eigenvalue are on the unit circle for frequencies that lie in the "transmission band", i.e.: $\{\eta :\ 0 \le \eta \le \eta_{lim} := \frac{\sqrt{5}}{2}\}$ while the third and fourth eigenvalue are real-valued. For frequencies higher than this limiting frequency, all eigenvalues are real-valued:

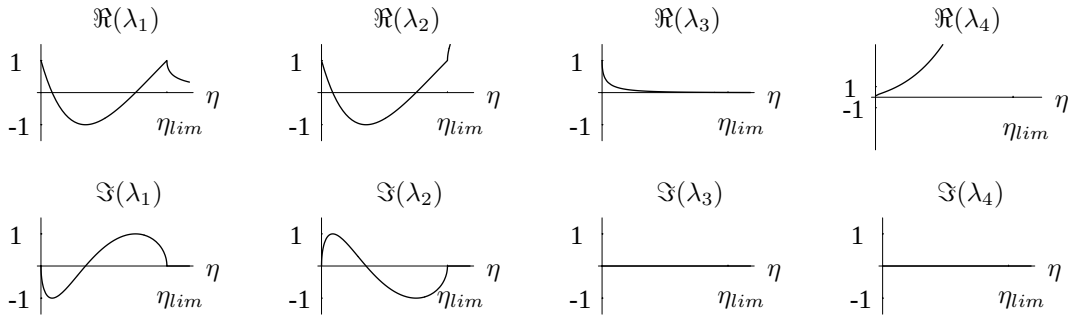

Figure 7: Eigenvalues of the Transfer Matrix **T** as a Function of the Normalized Frequency, η

A physical interpretation can be given by thinking of a chain where the left end is excited with a constant frequency while the right end is situated in infinity (i.e. any reflection from the right end is damped away and do not interfere with the incoming waves). For frequencies in the transmission band, undamped waves travel from left to right, while for higher frequencies wave propagation does not exist.

It is reasonable to introduce the following transformations:

$$\lambda_1 \quad = e^{-g_1} \;\Rightarrow\; \lambda_2 = e^{g_1} \tag{15}$$
$$\lambda_3 \quad = e^{-g_2} \;\Rightarrow\; \lambda_4 = e^{g_2} \tag{16}$$

with $\Re(g_k)$ defining the spacial decrease of amplitude and $\Im(g_k)$ defining the phase and the transition delay time. All eigenvectors are linearly independent for nearly all frequencies and can thus be used to construct a basis of the four-dimensional state space:

$$\mathbf{z}_n(t) = \sum_{k=1}^{4} p_n^k(t)\mathbf{z}_k^E(\eta)\,. \tag{17}$$

The boundary conditions considered imply that the state vector of this chain lies in the plane defined by the first two eigenvectors only:

$$\mathbf{z}_n = p_n^1(t)\mathbf{z}_1^E(\eta) + p_n^2(t)\mathbf{z}_2^E(\eta). \tag{18}$$

On the other hand a second implication also follows from the specific boundary conditions:

$$\sin(\Im(g_1)\tilde{N}) = 0 \;\Leftrightarrow\; \Im(g_1) = \frac{k\pi}{\tilde{N}},\; k \in \mathbb{Z}\,. \tag{19}$$

The first implication shows why the compression in the frequency spectrum can be interpreted as a (numerical) dispersion error:

$$\mathbf{z}_{n+1}(t) = \mathbf{T}(\eta)\mathbf{z}_n(t) = \mathbf{z}_n(t - t_d), \quad t_d(\eta) = \frac{\Im(g_1)(\eta)}{\eta}\,\frac{1}{\omega_c}\,. \tag{20}$$

The state at node n is imitated at node n+1 some delay time t_d later. Therefore, we can define an averaged phase velocity $v_p(\eta) = \frac{\ell}{t_d(\eta)}$, which depends on the normalized frequency. This dispersion effect has two origins: the investigated continuum itself possesses natural dispersion which is superposed by an additional, numerical dispersion. The following graphic shows a comparison of the (normalized) delay time $\tau := \omega_c t_d = \frac{\Im(g_1)(\eta)}{\eta}$ over the (normalized) frequency η, both for the continuum (solid line) and the discontinuum (dashed line):

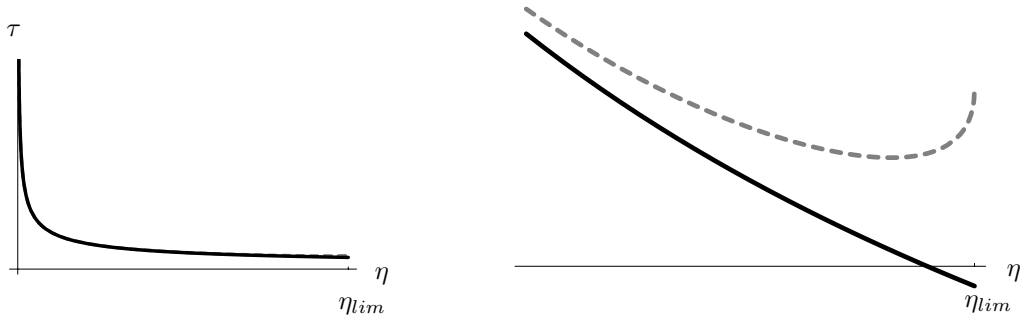

Figure 8: Qualitative Diagram of Delay Time τ: Continuum vs. Discontinuum. On the left side with respect to the whole frequency domain, on the right side in the region near the limiting frequency with strongly enlarged scales.

When looking at the whole transmission band (left figure), the approximation of the discontinuous chain looks fine. But near the limiting frequency (right figure) one notices a different behaviour caused by the additional numerical dispersion. When we expand the delay time τ of the discontinuum in a TAYLOR-series about the point $\eta = 0$, the

first term represents the exact delay time of the continuum. Thus the discretization error of this MBS-model can be approximated by the second term which is proportional to $\eta^{1.5}$.
(19) and (18) can be used to determine the $2\tilde{N}$ eigenfrequencies $\omega^E = \omega_c \eta^E$ of the MBS chain:

$$\eta_m^E = \begin{cases} \sqrt{\frac{-40\left(2+\cos(\frac{m\,\pi}{\tilde{N}})\right)+\sqrt{50}\sqrt{1+\cos(\frac{m\,\pi}{\tilde{N}})}\left(11+\cos(\frac{m\,\pi}{\tilde{N}})\right)}{32\ (-7+\cos(\frac{m\,\pi}{\tilde{N}}))}} & m = 1,\ldots,\tilde{N} \\ \sqrt{\frac{-40\left(2+\cos(\frac{m\,\pi}{\tilde{N}})\right)-\sqrt{50}\sqrt{1+\cos(\frac{m\,\pi}{\tilde{N}})}\left(11+\cos(\frac{m\,\pi}{\tilde{N}})\right)}{32\ (-7+\cos(\frac{m\,\pi}{\tilde{N}}))}} & m = \tilde{N}+1,\ldots,2\tilde{N} \end{cases} . \tag{21}$$

Using L'HOSPITAL's rule four times, (21.1) can be used to calculate the following limit:

$$\lim_{\tilde{N}\to\infty} (\omega_c \eta_m^E) = \pi^2 \sqrt{\frac{K_B}{m_x L^4}}\, m^2 = \omega_m^E, \tag{22}$$

see (3), showing the convergence towards the continuous beam.
When analyzing (21) for eigenfrequencies η^E near η_{lim}, we substitute $x := \frac{m}{2\tilde{N}},\ x \in (0,1]$. The derivative of (21.2) with respect to x has a simple root for x = 1, explaining (mathematically) why the (discrete) lines of the spectrum are compressed near the highest eigenfrequency.
Finally, we renormalize the frequency ω with the lowest eigenfrequency of the continuous beam:

$$\tilde{\eta} = \frac{\omega}{\tilde{\omega}_c},\ \tilde{\omega}_c = \pi^2 \sqrt{\frac{K_B}{m_x L^4}} \tag{23}$$

$$\Rightarrow\ \tilde{\eta} = \frac{32}{\pi^2}\sqrt{\frac{3}{5}}\,\tilde{N}^2\,\eta\,, \tag{24}$$

enabling us to compare the results of the MBS model to the following FEM model.

2.2 FEM Discretization

Now we want to present the results of a different method of discretization using finite elements of length ℓ based on HERMITE polynomials:

$$\begin{array}{ll} H_1(\xi) = 1 - 3\xi^2 + 2\xi^3 & H_2(\xi) = -\xi + 2\xi^2 - \xi^3 \\ H_3(\xi) = 3\xi^2 - 2\xi^3 & H_4(\xi) = \xi^2 - \xi^3 \end{array} \quad , \xi := \frac{x}{\ell} \tag{25}$$

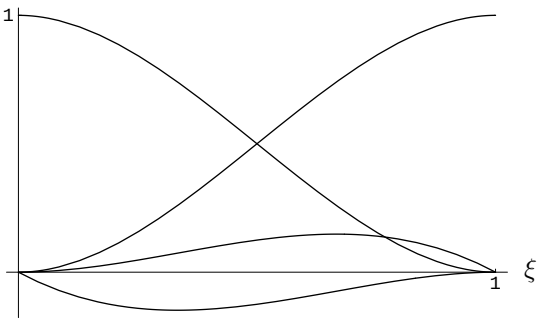

Figure 9: HERMITE Polynomials $H_1 - H_4$

These polynomials are chosen for a physical reason as they represent the exact solution of the PDE (1) for an element of the continuous beam charged with (generalized) forces on its boundary only in the static case. From the point of view of the associated variational problem, they are consistent with the essential boundary conditions.

With a separation ansatz using the same coordinates as before (see (3)),
$w(x,t) = \{H_1(\xi), H_2(\xi), H_3(\xi), H_4(\xi)\}\ \mathbf{q}_n(t)$, the equation of motion can be derived from (1) or by regarding the balance of energy:

$$\mathbf{M}_{FEM}\ddot{\mathbf{q}}_n + \mathbf{K}_{FEM}\mathbf{q}_n = \mathbf{F}_e\ . \tag{26}$$

Comparing this result to (4), the only (mathematical) difference is a different mass and stiffness matrix:

$$\mathbf{M}_{FEM} = \frac{m_x \ell}{420}\begin{pmatrix} 156 & -22 & 54 & 13 \\ -22 & 4 & -13 & -3 \\ 54 & -13 & 156 & 22 \\ 13 & -3 & 22 & 4 \end{pmatrix}, \tag{27}$$

$$\mathbf{K}_{FEM} = \frac{K_B}{\ell^3}\begin{pmatrix} 12 & -6 & -12 & -6 \\ -6 & 4 & 6 & 2 \\ -12 & 6 & 12 & 6 \\ -6 & 2 & 6 & 4 \end{pmatrix}, \tag{28}$$

while the main physical difference is that the FEM model has a potential energy which is spread along the beam continuously and not concentrated in "points" as in the case of the MBS model. Because of this mathematical analogy, the same calculations can be carried out. For a number of $\tilde{N}$ (FEM)-elements, the eigenfrequencies are:

$$\tilde{\eta}_m^E = \begin{cases} \frac{2\sqrt{30}}{\pi^2}\tilde{N}^2\sqrt{\frac{411+222\ \cos(\frac{m\,\pi}{\tilde{N}})-3\ \cos(\frac{2\,m\,\pi}{\tilde{N}})-f(\frac{m}{\tilde{N}})}{131-72\ \cos(\frac{m\,\pi}{\tilde{N}})+\cos(\frac{2\,m\,\pi}{\tilde{N}})}} & m = 1,\ldots,\tilde{N}-1 \\ \frac{2\sqrt{30}}{\pi^2}\tilde{N}^2\sqrt{\frac{411+222\ \cos(\frac{m\,\pi}{\tilde{N}})-3\ \cos(\frac{2\,m\,\pi}{\tilde{N}})+f(\frac{m}{\tilde{N}})}{131-72\ \cos(\frac{m\,\pi}{\tilde{N}})+\cos(\frac{2\,m\,\pi}{\tilde{N}})}} & m = \tilde{N},\ldots,2\tilde{N} \end{cases} \tag{29}$$

$$f(\frac{m}{\tilde{N}}) = \sqrt{6}\sqrt{30380 + 33026\ \cos(\frac{m\,\pi}{\tilde{N}}) + 2723\ \cos(\frac{2\,m\,\pi}{\tilde{N}}) + 22\ \cos(\frac{3\,m\,\pi}{\tilde{N}}) - \cos(\frac{4\,m\,\pi}{\tilde{N}})}\ ,$$

using the normalization (23).
Finally, we want to visualize the results for a 64 element model which has 128 degrees of freedom:

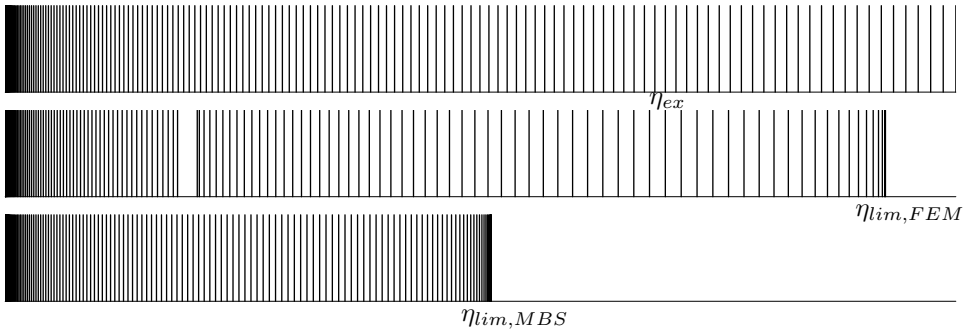

Figure 10: Frequency Spectra: Continuum, FEM, MBS

The first graphic is an excerpt of the spectrum of the continuous beam: the distance between two adjacent eigenfrequencies grows for increasing modes. The next spectrum is based on the FEM discretization. The calculated eigenfrequencies are compressed near the highest frequency, $\eta_{lim,FEM}$ which is higher than the exact 128th eigenfrequency, η_{ex}. Another interesting property of the FEM spectrum is the gap for modes numbers approximately half of the degree of freedom. We did not succeed to explain this gap yet but we could find the values of the cut-off-frequencies analytically. The last spectrum is based on the MBS model. The lines approaching $\eta_{lim,MBS}$ are also compressed but the highest calculated frequency is smaller than η_{ex}.

Another way of visualizing the results is to divide the eigenfrequencies $\tilde{\eta}_m^E$ by their mode, m. The continuum is then represented by a straight line while both discontinua drift away from this line for higher modes:

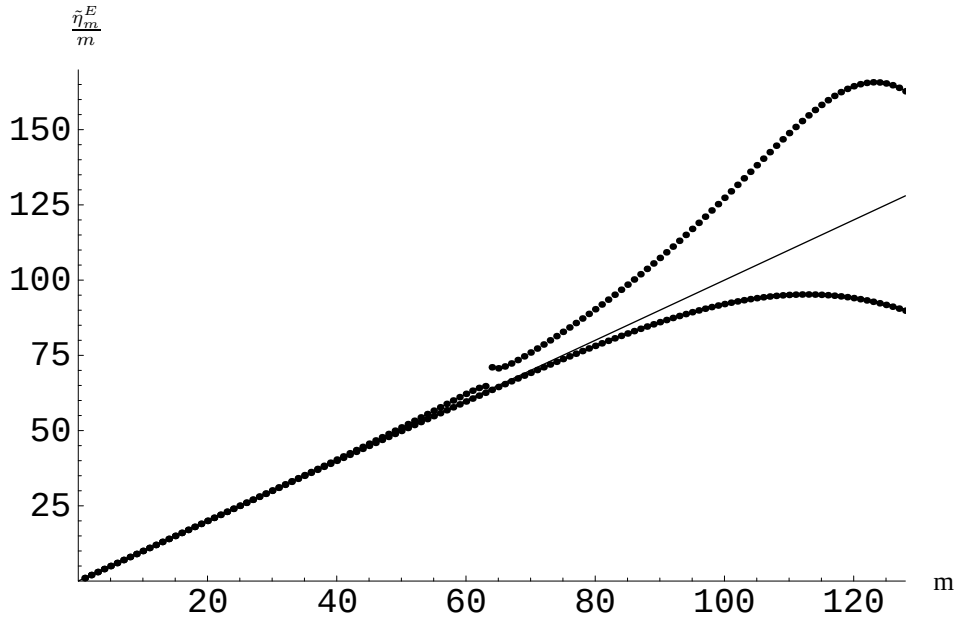

Figure 11: Visualization of the Results of the 64 Elements Model: $\tilde{\eta}_m^E$ = normalized frequency, m = mode number

For low frequencies, both discontinua cannot be distinguished from the exact solution for the continuum. For higher frequencies, the FEM results lie above the exact eigenfrequencies, which seems to be typical for finite elements. Again you can see the gap, which is associated with the middle modus, ($m = \tilde{N}$).
The MBS results stay somewhat closer to the exact solution before drifting away to eigenfrequencies which are too small. The maxima in the graphs related to discontinua follow from the special choice of the ordinate scale.

Finally, let us have a look at the modal density distributions of the continuum, the FEM-model and the MBS-model. For a number of elements of 512 for both models, we divide the frequency range of the FEM-model into 70 equidistant intervals and plot the number of eigenfrequencies in one interval over the frequency axis:

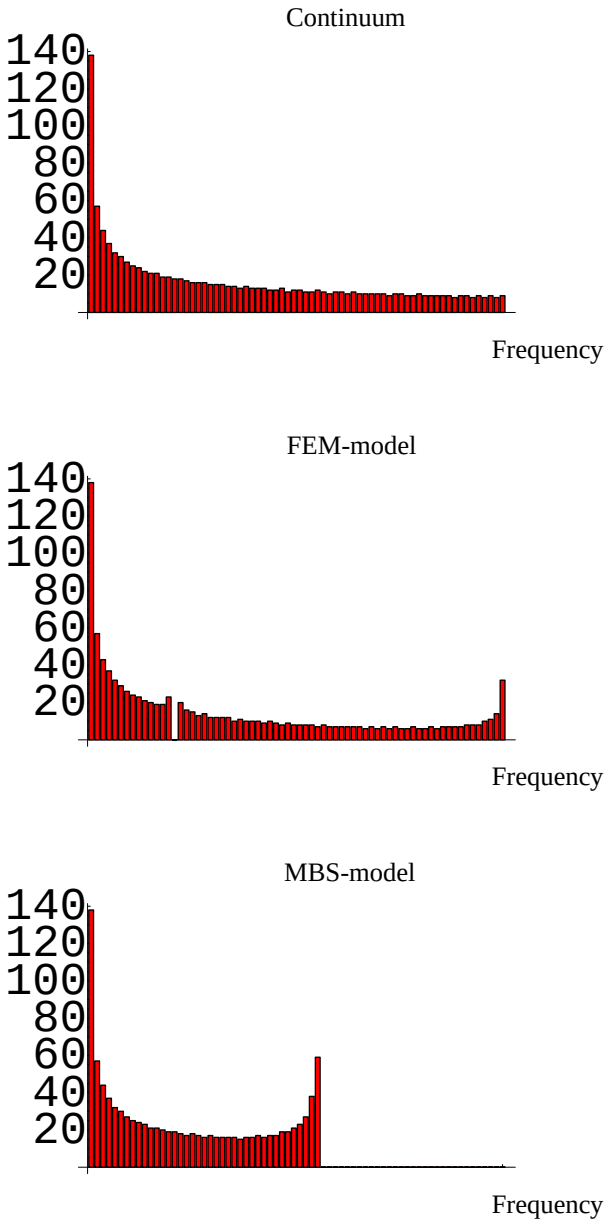

Figure 12: Modal Density Distribution of the Straight Beam, Continuum, FEM-Model, MBS-Model, 512 Elements

The frequency distribution for small frequencies is the same for all three plots. At the right end, both discrete models have a similar compression and again you can see the gap in the frequency spectrum of the FEM-model.

3 Conclusions

In this paper we demonstrated that a certain systematic error occurs whenever a continuous system is solved numerically using finite methods. This error affects the distribution of eigenfrequencies, causing an additional *numerical dispersion error*. In the associated frequency spectra, the lines approaching the highest eigenfrequency of the discrete systems are compressed. This was first observed *numerically* for bending oscillations of a ring structure under various boundary conditions. Here we show *analytically* that this compression occurs also in bending oscillations of the straight beam, regardless of the discretization method used. When analyzing the results of a FEM-model, we discovered that besides this compression at the end of the spectra, there are two other compression points which form a gap in the frequency spectrum. The gap occurs for mode numbers which are approximately half of the degree of freedom. We could calculate the cut-off-frequencies for this gap but could not explain the physics of its existence.
The authors are aware that for increasing mode numbers, the approximation of a continuum with discrete models becomes worse, for a fixed number of elements. Eventually, the dynamical behaviour of the model has very little to do with that of the continuous system. Therefore, when looking at continuous systems, our results can help to understand certain systematic errors in the frequency spectrum *qualitatively*. For the MBS-model, which one could easily materialize, the results are also *quantitatively* correct.

Literature

1. Brepta, R.; Valeš, F.; Cerv, J.; Tikal, B.: Rayleigh wave dispersion due to spatial (FEM) discretization of a thin elastic solid having non-curved boundary. Computer and Structures. Vol. 58, No.6, August (1994), 1233-1244.
2. Brillouin, L.: Wave propagation in periodic structures: electric filters and crystal lattices. Dover Publications, Inc., 2. Edition, (1953).
3. Brunk, G.; Weckner, O.: Dispersion als Diskretisierungsfelder bei der Untersuchung von Balkenschwingungen, dargestellt am Beispiel eines MKS-Modelles des geraden Biegebalkens. Festschriftbeitrag für Herrn Prof. Dr.-Ing. H. Sander, ISBN: 3-7983-1866-2, Juni (2001).
4. Cherukuri, H.P.: Dispersion analysis of numerical approximations to plane wave motions in an isotropic elastic solid. Computational Mechanics, Volume 25, Issue 4, October (1999), 317-328.
5. Rao, K. R.; Nehrbass, J.; Lee, R.: Discretization errors in finite methods: issues and possible solutions. Computational methods in applied mechanics and engineering, Elsevier Science SA, Lausanne, February (1999).
6. Rint, C. (Editor): Handbuch für Hochfrequenz- und Elektrotechniker. Verlag für Radio-, Foto-, Kinotechnik, Berlin, 1. Edition, Vol. 1, (1981), 205 Seiten.
7. Weckner, O.: Die antimetrischen bzw. asymmetrischen Eigenschwingungszustände eines MKS-Modelles eines Kreisrings bei verschiedenen Lagerungen. Diplomarbeit von O. Weckner, Betreuung durch Herrn Prof. G. Brunk, Universitätsbibliothek der TU Berlin, Abteilung Luft- und Raumfahrt, Signatur: 4Qg4691, Dezember (2000).

Address: Dipl.-Ing. Olaf Weckner, olaf@weckner.de, Prof. Dr.-Ing. Gerd Brunk, gerd.brunk@tu-berlin.de, Institut für Mechanik, M244, Technische Universität Berlin, Straße des 17. Juni 135, 10623 Berlin, Germany.